International Conference on Power, Electronics, Communications, Computing, and Intelligent Infrastructure 2026 (PECCII), 17-18 June 2026, PUST, Pabna, Bangladesh

2026 International Conference on Power, Electronics, Communications, Computing, and Intelligent Infrastructure (PECCII) | 979-8-3195-3395-1/26/$31.00 ©2026 IEEE | DOI: 10.1109/PECCII70991.2026.11661867

DFT-spread Affine Frequency Division Multiplexing for Transmission over Doubly Dispersive Channels

Sahal Hossain Siam
ECE Discipline
Khulna University
Khulna-9208, Bangladesh
Email: msc250915@ku.ac.bd

Mohammad Ismat Kadir
ECE Discipline
Khulna University
Khulna-9208, Bangladesh
Email: ismat.kadir@ece.ku.ac.bd

***Abstract*—Affine Frequency Division Multiplexing (AFDM) has recently attracted substantial attention as a promising modulation scheme for high-mobility wireless environments because of its resilience to doubly dispersive channel effects. In this paper, we propose a DFT-spread AFDM framework and evaluate its effectiveness in mitigating impairments caused by doubly selective channels and in reducing the peak-to-average power ratio (PAPR). A detailed system model is developed, supported by mathematical analysis and comprehensive simulation studies. The performance of the proposed DFT-spread AFDM scheme is compared with conventional OFDM and OTFS waveforms. Simulation results show that DFT-spread AFDM significantly reduces the bit error rate (BER) across a wide range of signal-to-noise ratios (SNRs), primarily due to enhanced frequency diversity and lower PAPR. These gains are supported by comparative BER curves for conventional AFDM and DFT-spread AFDM, together with the corresponding PAPR evaluations. These findings highlight the suitability of DFT-spread AFDM for high-mobility applications, such as UAV-assisted and railway communication systems, characterized by doubly selective channel conditions.**

***Index Terms*—AFDM, OFDM, OTFS, DFT-spreading, doubly selective channel.**

I. Introduction

Wireless communication in high-mobility contexts—such as high-speed trains, vehicular networks, satellite links, and developing UAV-assisted systems—experiences significant performance deterioration due to doubly selective channels, characterized by variations in both delay and Doppler effects [1]. In these circumstances, swift channel variations cause inter-symbol interference (ISI) and inter-carrier interference (ICI), which considerably distort the transmitted signal and elevate the bit error rate (BER). Traditional multicarrier systems, such as orthogonal frequency-division multiplexing (OFDM), are well-known for their spectrum efficiency and straightforward equalization. Nevertheless, their orthogonality is particularly susceptible to frequency shifts generated by Doppler effects. Moderate Doppler spread disrupts the orthogonality of subcarriers, leading to significant inter-carrier interference (ICI) and substantial bit error rate (BER) deterioration, particularly in 5G/6G mobility contexts and high-frequency millimeter wave bands.

To overcome these restrictions, modulation methods that operate in the delay-Doppler (DD) domain—particularly orthogonal time–frequency space (OTFS) [2], [3] and recently developed affine frequency division multiplexing (AFDM)—have emerged as viable alternatives [4]–[6]. OTFS translates QAM symbols into the delay-Doppler domain using a symplectic Fourier transform, resulting in a channel representation that remains practically time-invariant even at elevated mobility [3], [7]. This characteristic facilitates enhanced equalization and resilience to Doppler spread. However, the implementation of OTFS entails two-dimensional transformations and considerable pilot overhead, which can potentially increase complexity in practical systems [2].

AFDM has attracted interest as a contemporary solution for doubly dispersive channels. AFDM employs affine Fourier transformations with chirp-based basis functions, resulting in waveforms that inherently disperse across both time and frequency [4]. This chirp structure inherently enhances robustness in doubly selective channels, delivering a wide variety and superior resilience to both delay and Doppler spreads. Furthermore, AFDM has a more sparse and organized channel matrix, thus decreasing implementation complexity and enabling low-complexity equalization. Recent studies have shown that AFDM outperforms OFDM and OTFS in rapidly fluctuating channels, prompting further exploration for future 6G systems [5], [6]. As a further advance, Li et al. [8] presented a RIS-assisted AFDM system, demonstrating that the discrete affine Fourier transform (DAFT) architecture intrinsically offers Doppler variety and resilience in rapidly fluctuating channels. Kwon et al. [9] demonstrated that soft-information detection for AFDM in MIMO dispersive channels can substantially decrease BER, even in the presence of channel estimate errors. Additionally, Tek and Basar [10] introduced a secure AFDM architecture for extreme-mobility settings, demonstrating that AFDM offers complete diversity gain and enhanced robustness compared to traditional OFDM waveforms.

Simultaneously, DFT spreading — commonly used in OFDM systems, namely single-carrier frequency-domain equalization (SC-FDE) or single-carrier frequency-division multiple access (SC-FDMA) — offers additional advantages. These include a reduced peak-to-average power ratio (PAPR) and enhanced frequency diversity. [11], [12] The integration of DFT spreading with OFDM produces a hybrid approach, termed DFT spread OFDM, which preserves the benefits of

979-8-3195-3395-1/26/$31.00 ©2026 IEEE
Authorized licensed use limited to: Khulna University. Downloaded on October 13,2026 at 09:49:18 UTC from IEEE Xplore. Restrictions apply.

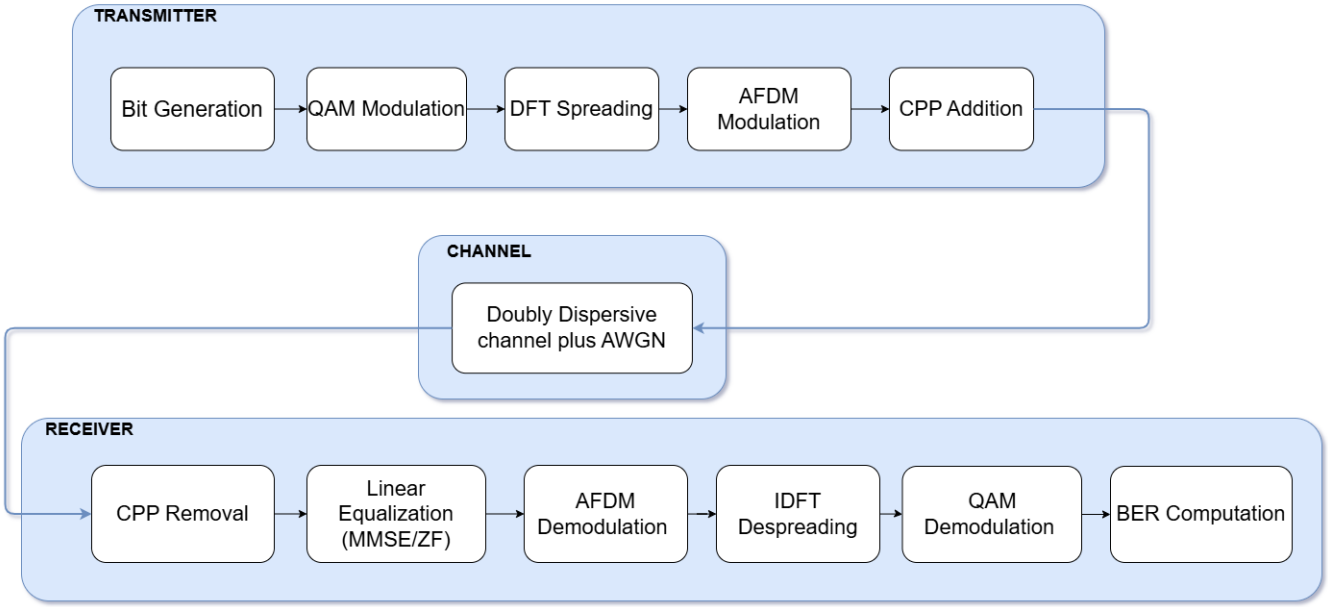


Fig. 1. Block diagram of DFT-spread AFDM system.

both methods: reduced PAPR, significant Doppler resilience, and improved robustness in multipath environments. Specifically, SC-FDMA is a strong contender for uplink-focused applications and power-constrained devices in next-generation networks [13].

Inspired by these benefits, this work presents a comprehensive end-to-end DFT-spread AFDM transceiver that includes AFDM modulation/demodulation, CPP addition/removal, and MMSE equalization. To assess its performance, we performed a rigorous and thorough comparison with DFT-spread OFDM and DFT-spread OTFS, using similar simulation parameters. These include the same Rayleigh delay-Doppler channel realizations, QAM order, subcarrier spacing, frame count, and SNR range (0–16 dB). The aim is to measure the BER reduction provided by AFDM compared to OTFS and OFDM in demanding high-mobility settings.

The contributions of this study can be summarized as follows:

1) A comprehensive DFT-spread AFDM system architecture has been designed, modeled, and simulated, encompassing intricate channel modeling and equalization.
2) A comprehensive BER comparison is conducted between AFDM, OTFS, and OFDM, utilizing identical parameters to ensure equity.
3) Simulation results indicate that DFT-spread AFDM attains markedly enhanced BER performance, particularly at moderate and high SNR levels, corroborating its superiority in doubly selective wireless channels.

The study presents compelling evidence that DFT-spread AFDM is a viable waveform for next-generation mobility-centric applications with the aid of comprehensive simulations and analyses [13]. These applications include high-speed rail communication, vehicular networks, satellite links, and integrated sensing and communication systems.

The rest of the paper is organized as follows: In Section II, we present the proposed DFT-spread AFDM system model, outlining the system's transceiver architecture and the channel model considered. Section III presents the simulation results. The limitations of this study and potential future work are described in Section IV. Finally, Section V concludes the article.

II. SYSTEM OVERVIEW

The comprehensive design of the proposed DFT-spread AFDM system is illustrated in Fig. 1. The transmitter employs QAM modulation to map the information bits, followed by DFT spreading and AFDM modulation. A chirp-periodic prefix (CPP) is applied before transmission across a multipath Rayleigh fading channel, which is characterized by Doppler shifts and additive white Gaussian noise (AWGN). At the receiver, the CPP is removed first, followed by linear equalization (MMSE/ZF), and AFDM demodulation. The resulting demodulated symbols are then subjected to IDFT-based despreading operation, and finally, the despread symbols are mapped to the output bits using QAM demodulation.

A. Transmitter Processing

The transmission process of the proposed DFT-spread AFDM system begins with the generation of a binary information sequence, which is mapped into complex modulation symbols using 4-QAM, resulting in a normalized symbol vector $x[n]$, where $n = 0, 1, \ldots, (N_{\mathrm{d}} - 1)$. Specifically, for example, the system employs a total of $N = 64$ transmission samples per frame, where $N_{\mathrm{d}} = 61$ data samples are used and

Authorized licensed use limited to: Khulna University. Downloaded on October 13,2026 at 09:49:18 UTC from IEEE Xplore. Restrictions apply.

$\text{CPP}_\ell = 3$ samples are reserved for the CPP, matching the maximum discrete delay index of the channel.

To reduce peak-to-average power ratio and improve robustness in dispersive fading channels, the QAM symbols undergo DFT spreading. This operation transforms the input vector into

$$\begin{aligned} X[k] &= \text{DFT}_{N_\text{d}}\left(x[n]\right) \\ &= \sum_{n=0}^{(N_\text{d}-1)} x[n]\, e^{-j\frac{2\pi kn}{N_\text{d}}}, \end{aligned} \tag{1}$$

where $\text{DFT}_{N_\text{d}}(\bullet)$ represents the $N_\text{d}-$point discrete Fourier transform, which produces frequency-domain symbols $X[k]$ from the time-domain symbols $x[n]$.

Following DFT spreading, AFDM modulation is performed by applying a quadratic chirp. Each DFT-spread symbol is mapped to the time domain using

$$s[n] = X[n]\, e^{j2\pi c_1 n^2},$$

where the chirp parameter is given by

$$c_1 = \frac{2(k_{\max} + k_v) + 1}{2N_\text{d}},$$

with $k_{\max} = 4$ representing the maximum Doppler index and $k_v = 1$ serving as a guard parameter. The chirp-based modulation causes each sample $s[n]$ to occupy a wider Doppler footprint, enabling improved resilience in high-mobility channels.

To ensure circular convolution compatibility and allow the channel to be represented by a structured matrix, a CPP is appended. The CPP samples are generated as

$$\text{CPP}[m] = s\big[N_\text{data} - \text{CPP}_\ell + m\big]\, e^{-j2\pi c_1\left(N^2 + 2N(-\text{CPP}_\ell + m)\right)},$$

where the exponential term preserves the continuity of the AFDM chirp. The final transmitted signal is

$$S_\text{CPP} = \begin{bmatrix} \text{CPP} \\ s \end{bmatrix}.$$

The peak-to-average power ratio (PAPR) of the transmitted block S_CPP is defined as

$$\text{PAPR} \triangleq \frac{\max\limits_{0\le n\le N-1} |S_\text{CPP}[n]|^2}{\frac{1}{N}\sum\limits_{n=0}^{N-1} |S_\text{CPP}[n]|^2}.$$

The complementary cumulative distribution function (CCDF) of PAPR is computed as

$$\text{CCDF}(\gamma) \triangleq \Pr\{\text{PAPR} > \gamma\}.$$

This vector is passed through a doubly selective delay–Doppler Rayleigh fading channel characterized by complex gains h_i, discrete delays τ_i, and Doppler shifts $f_{D,i} = \frac{k_i}{NT}$, where k_i denotes the Doppler index.

The received sample can then be expressed as:

$$r[n] = \sum_{i=1}^{9} h_i\, s_\text{CPP}[n - \tau_i]\, e^{-j2\pi f_{D,i} n} + \omega[n],$$

which captures both delay-induced ISI and Doppler-induced ICI, while $\omega[n]$ indicates the additive white Gaussian noise (AWGN).

B. Receiver Mechanism

The receiver begins by collecting the symbols $r[n]$ received from the channel. The first operation in the receiver is the removal of the CPP, which extracts the N_d-length symbol vector r in the receiver of AFDM.

Different types of detectors can be applied at the receiver of the proposed system. The simplest of these detectors is the linear detector, namely the zero-forcing (ZF) or the minimum mean squared error (MMSE) detector.

To compensate for distortions introduced by the doubly selective channel, the ZF detector employs the weight matrix given by:

$$\mathbf{W}_\text{ZF} = \left(\mathbf{H}^H\mathbf{H}\right)^{-1}\mathbf{H}^H,$$

and the ZF-based symbol estimate is obtained as

$$\hat{\mathbf{s}}_\text{ZF} = \mathbf{W}_\text{ZF}\mathbf{r}.$$

However, the ZF detector experiences an inherent noise enhancement. As a remedy, an MMSE equalizer is employed, designed specifically for the AFDM channel matrix structure. The AFDM channel matrix $\mathbf{H}$ is constructed using the estimated or known multipath components, where each entry reflects combined delay and Doppler effects. Equalization is performed using

$$\mathbf{W}_\text{MMSE} = \left(\mathbf{H}^H\mathbf{H} + \sigma^2\mathbf{I}\right)^{-1}\mathbf{H}^H,$$

and the equalized signal is obtained as

$$\hat{s} = \mathbf{W}_\text{MMSE}\, r.$$

AFDM demodulation removes the chirp component applied during modulation using the inverse transformation

$$\hat{X}[n] = \hat{s}[n]\, e^{-j2\pi c_1 n^2}.$$

The result is a chirp-free sequence in the equivalent frequency domain. To recover the original QAM symbols, an IDFT-based despreading operation is applied:

$$\hat{x}[n] = \frac{1}{N_\text{d}} \sum_{k=0}^{(N_\text{d}-1)} \hat{X}[k]\, e^{j\frac{2\pi kn}{N_\text{d}}},$$

which reconstructs the original low-PAPR single-carrier structure.

Finally, the demodulated symbols are mapped back to the estimated bits using the corresponding constellation.

Authorized licensed use limited to: Khulna University. Downloaded on October 13,2026 at 09:49:18 UTC from IEEE Xplore. Restrictions apply.

TABLE I
SIMULATION PARAMETERS

Parameter	Value
Modulation	4-QAM
Number of Subcarriers (N)	64
Subcarrier Spacing (Δf)	15 kHz
Symbol Duration (T)	$1/\Delta f$
Channel Type	9-tap Rayleigh fading channel
Number of Channel Taps (P)	9
Maximum Delay Index ($l_{\max}$)	3
Maximum Doppler Index ($k_{\max}$)	4
Equalizer	Linear (MMSE/ZF)
SNR Range	0–16 dB (step 2 dB)
CPP Length (L_{CPP})	$\max(\ell_i)$
Number of Data Symbols (N_{d})	$N - L_{\mathrm{CPP}}$
Guard Parameter (k_v)	1
Doppler Parameter (c_1)	$\frac{2(\max(k_i)+k_v)+1}{2N_{\mathrm{d}}}$
AFDM Parameter (c_2)	$1/N_{\mathrm{d}}^2$
Number of Frames (N_{frame})	200000

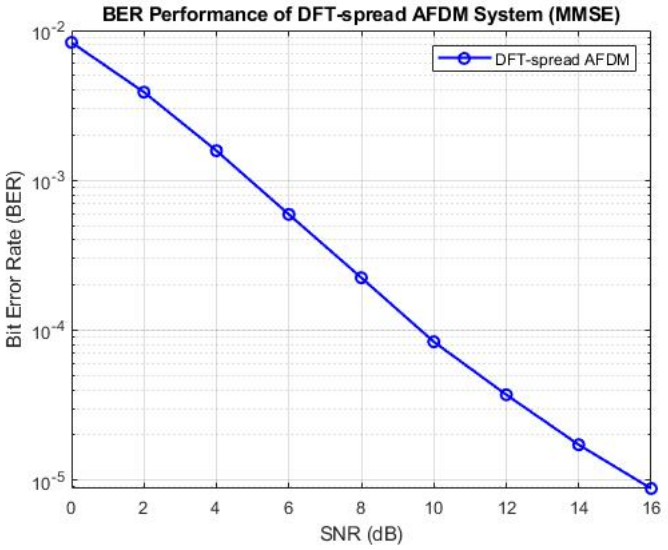


Fig. 2. DFT-spread AFDM with MMSE over doubly selective channel

III. RESULTS AND DISCUSSION

We have investigated the BER and PAPR performance of the proposed DFT-spread AFDM system using the parameters listed in Table I. To be specific, the system employs 4-QAM modulation over $N = 64$ subcarriers with a subcarrier spacing of $\Delta f = 15$ kHz, yielding a symbol duration $T = 1/\Delta f$. A 9-tap Rayleigh fading channel is considered to model doubly dispersive propagation, characterized by a maximum delay index $l_{\max} = 3$ and a maximum Doppler index $k_{\max} = 4$. In other words, we use discrete delays $\tau_i \in [0, 3]$, and Doppler shifts $f_{D,i} = \frac{k_i}{NT}$, where $k_i \in [-4, 4]$ for our investigations.

At the receiver, linear zero-forcing (ZF) and minimun mean-square error (MMSE) equalizers are applied to mitigat channel-induced interference. The signal-to-noise ratio (SNR is varied from 0 to 16 dB in steps of 2 dB. A CPP of lengt $L_{\mathrm{CPP}} = \max(\ell_i)$ is employed, resulting in $N_{\mathrm{d}} = N - L_{\mathrm{CPI}}$ data symbols per AFDM block.

To ensure robustness against Doppler spread, a guard pa rameter $k_v = 1$ is introduced. The AFDM design parameter are selected as

$$c_1 = \frac{2(\max(k_i) + k_v) + 1}{2N_{\mathrm{d}}}, \qquad c_2 = \frac{1}{N_{\mathrm{d}}^2},$$

which guarantees orthogonality of the AFDM basis functions under the considered channel conditions. All results are obtained by averaging over 200,000 Monte Carlo frames to ensure statistical reliability of the BER and PAPR performance.

A. Error Performance

Figure 2 illustrates the BER performance of the proposed DFT-spread AFDM system with MMSE equalization over the doubly selective delay–Doppler channel. The curve decreases almost linearly on the logarithmic scale, showing that the scheme benefits steadily from every increase in SNR. At 0 dB the BER is 8.31×10^{-3}, which is reasonable for such a harsh channel. When the SNR is raised to 4 dB and 8 dB, the BER drops to 1.58×10^{-3} and 2.20×10^{-4}, respectively. For higher SNR values, the performance continues to improve: it reaches 8.0×10^{-5} at 10 dB, 4.0×10^{-5} at 12 dB, 2.0×10^{-5} at 14 dB, and finally 1.0×10^{-5} at 16 dB. Overall, this figure confirms that the DFT-spread AFDM waveform, in combination with MMSE equalization, can effectively exploit the available delay–Doppler diversity and provide very reliable communication over the considered SNR range.

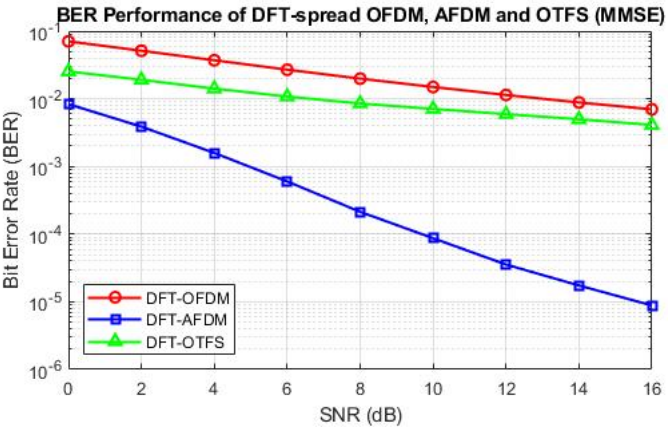


Fig. 3. BER comparison of DFT-spread OFDM, DFT-spread OTFS, and DFT-spread AFDM using MMSE equalization over a doubly selective channel.

Figure 3 presents a BER comparison of three DFT-spread systems, namely DFT-spread OFDM, DFT-spread AFDM and DFT-spread OTFS, when all of them employ MMSE equalization. At low SNR (0 dB), DFT-spread OFDM exhibits the highest error rate, with a BER of 7.048×10^{-2}, reflecting its strong sensitivity to Doppler-induced interference. DFT-spread OTFS starts in the mid-10^{-2} region with a BER of 2.535×10^{-2}, while the proposed DFT-spread AFDM begins just below 10^{-2} at 8.34×10^{-3}. As SNR increases, the

Authorized licensed use limited to: Khulna University. Downloaded on October 13,2026 at 09:49:18 UTC from IEEE Xplore. Restrictions apply.

behavior of the three schemes diverges. The BER of DFT-spread OFDM decreases only gradually and remains in the 10^{-2} range up to 12 dB (e.g., 1.137×10^{-2}), before dropping below 10^{-2} at higher SNR, reaching 6.99×10^{-3} at 16 dB. DFT-spread OTFS improves more noticeably but stays within the 10^{-2} decade until 10 dB (e.g. 7.08×10^{-3}), and reaches 4.11×10^{-3} at 16 dB. In contrast, the DFT-spread AFDM curve shows a much steeper decline, reaching the 10^{-4} level by 8 dB with a BER of 2.10×10^{-4}, and continuing to improve to the 10^{-5} level at high SNR, down to 1.00×10^{-5} at 16 dB. This behavior highlights the benefit of combining AFDM with DFT-spreading under MMSE equalization for operation in doubly selective channels.

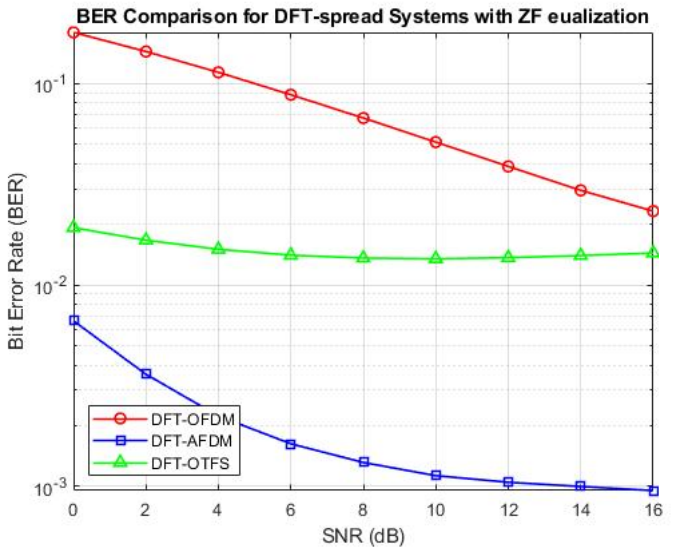


Fig. 4. BER comparison of DFT-spread OFDM, DFT-spread OTFS, and DFT-spread AFDM using ZF equalization over a doubly selective channel.

Figure 4 shows the BER performance of the same three DFT-spread systems when a ZF equalizer is applied at the receiver. In this case, all curves are shifted upwards compared to the MMSE scenario, because ZF does not take the noise power into account and therefore tends to enhance noise in deep fades. For DFT-spread OFDM, the BER starts above 10^{-1} at 0 dB and only slowly decreases, remaining around the high 10^{-2} region at 16 dB. The BER curve of DFT-spread OTFS is relatively flat, varying only slightly around the 10^{-2} level over the whole SNR range, which indicates that the benefit of increasing SNR is limited when ZF is used. The proposed DFT-spread AFDM still exhibits the most favourable trend: it begins below 10^{-2} at 0 dB and gradually decreases to around 10^{-3} at 16 dB. Even with the simpler ZF equalizer, the DFT-spread AFDM scheme maintains a clear robustness to the doubly selective channel and achieves noticeably lower BER than the other two DFT-spread waveforms.

The exceptional performance of AFDM is attributed to its modulation inside the affine Fourier transform domain, which inherently disperses symbol energy across both time and frequency. AFDM, when integrated with DFT spreading, improves multipath variety, diminishes peak-to-average power ratio (PAPR), and provides enhanced resilience against Doppler-induced distortions. Consequently, AFDM retains a BER advantage of roughly one order of magnitude over OFDM at moderate SNR values (6–10 dB) and consistently surpasses OTFS at elevated SNR levels. This comparative assessment validates AFDM as a remarkably resilient and efficient waveform option for next-generation high-mobility wireless communication systems.

B. PAPR Performance (CCDF Analysis)

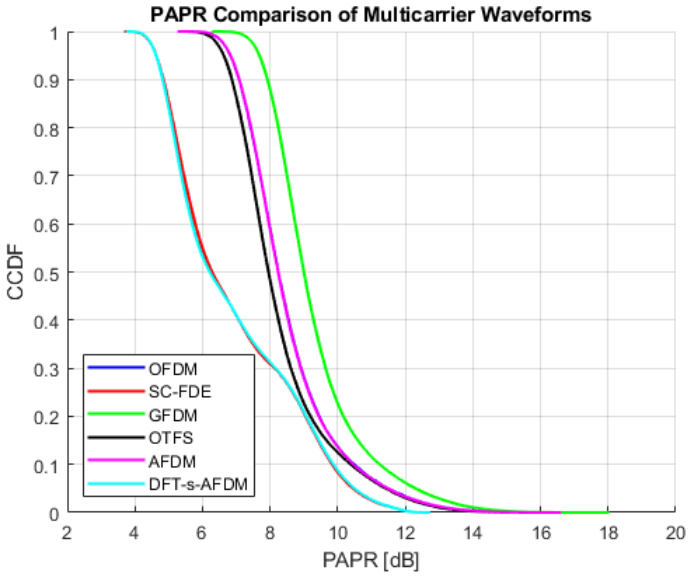


Fig. 5. CCDF of PAPR comparison for OFDM, SC-FDE, GFDM, OTFS, AFDM, and DFT-spread AFDM.

Figure 5 illustrates the PAPR CCDF for OFDM, SC-FDE, GFDM, OTFS, AFDM, and DFT-s-AFDM. The CCDF quantifies the probability that the instantaneous PAPR exceeds a given threshold; therefore, a leftward shift indicates improved PAPR performance. As observed, GFDM exhibits the highest PAPR distribution (right-most curve), whereas SC-FDE and DFT-s-AFDM achieve the lowest PAPR (left-most curves), highlighting the peak-reduction benefit of DFT spreading. OTFS and AFDM demonstrate intermediate PAPR behavior relative to the other waveforms. Notably, the proposed DFT-s-AFDM consistently attains the most favorable CCDF among the compared schemes, indicating improved amplifier-friendly transmission while preserving the underlying AFDM structure.

C. Comparison of the Proposed Scheme with Benchmarks

Table II provides a BER comparison of DFT-spread OFDM, DFT-spread OTFS, and the proposed DFT-spread AFDM under MMSE equalization at representative SNR values. At both 10 dB and 16 dB, the DFT-spread AFDM waveform achieves BERs that are two to three orders of magnitude lower than those of the OFDM- and OTFS-based counterparts. This clearly demonstrates the superior robustness of DFT-spread AFDM in doubly selective channels.

Authorized licensed use limited to: Khulna University. Downloaded on October 13,2026 at 09:49:18 UTC from IEEE Xplore. Restrictions apply.

TABLE II
BER SUMMARY UNDER MMSE EQUALIZATION

Waveform	BER at 10 dB	BER at 16 dB
DFT-spread OFDM	1.49×10^{-2}	6.99×10^{-3}
DFT-spread OTFS	7.08×10^{-3}	4.11×10^{-3}
DFT-spread AFDM	9.00×10^{-5}	1.00×10^{-5}

TABLE III
PAPR COMPARISON AT CCDF $= 10^{-3}$

Waveform	Relative PAPR
OFDM	Highest
OTFS	High
Conventional AFDM	Moderate
DFT-spread AFDM	Lowest

Table III summarizes the PAPR performance at a CCDF of 10^{-3}. The proposed DFT spread AFDM exhibits the lowest PAPR among all waveforms considered, confirming the peak-reduction benefit of DFT spreading. This improved PAPR behavior indicates enhanced power-efficiency and amplifier-friendly transmission, complementing the significant BER gains observed for DFT-spread AFDM.

IV. LIMITATIONS AND POTENTIAL FUTURE WORKS

This paper provides a rudimentary study of the proposed DFT-spread AFDM scheme. Linear MMSE and ZF receivers are considered here, which can be replaced by advanced receivers for improved performance. Additional future research directions include the integration of MIMO architectures with DFT-spread AFDM to further enhance spectral efficiency and reliability. Investigating low-complexity receiver designs and machine-learning-based channel estimation frameworks could significantly reduce computational burden while improving performance. Additionally, adaptive optimization of chirp and spreading parameters also remains an important avenue for maximizing performance under diverse and rapidly varying mobility conditions.

V. CONCLUSION

In this paper, we have proposed a DFT-spread AFDM for communication over doubly selective channels. Through detailed system modeling, numerical simulations, and comparative evaluation, we demonstrated that DFT-spread AFDM consistently outperforms conventional AFDM, OFDM, and OTFS waveforms. The combination of chirp-based Doppler robustness and DFT-induced diversity gain makes DFT-spread AFDM a highly reliable and efficient modulation technique for high-mobility scenarios. The results strongly indicate that DFT-spread AFDM is a promising candidate waveform for future 6G communication systems.

REFERENCES

[1] G. Taubock, F. Hlawatsch, D. Eiwen, and H. Rauhut, "Compressive estimation of doubly selective channels in multicarrier systems: Leakage effects and sparsity-enhancing processing," *IEEE Journal of Selected Topics in Signal Processing*, vol. 4, no. 2, pp. 255–271, 2010.

[2] R. Hadani, S. Rakib, M. Tsatsanis, A. Monk, A. J. Goldsmith, A. F. Molisch, and R. Calderbank, "Orthogonal time frequency space modulation," in *IEEE Wireless Communications and Networking Conference (WCNC)*, 2017.

[3] V. S. Bhat, S. G. Dayanand, and A. Chockalingam, "Performance analysis of OTFS modulation with receive antenna selection," *IEEE Transactions on Vehicular Technology*, vol. 70, no. 4, pp. 3382–3395, 2021.

[4] A. Bemani, N. Ksairi, and M. Kountouris, "AFDM: a full diversity next generation waveform for high mobility communications," in *IEEE International Conference on Communications (ICC) Workshops*, 2021, pp. 1–6.

[5] W. Benzine, A. Bemani, N. Ksairi, and D. Slock, "Affine frequency division multiplexing for communications on sparse time-varying channels," in *IEEE Global Communications Conference*, 2023, pp. 4921–4926.

[6] A. Bemani, N. Ksairi, and M. Kountouris, "Affine frequency division multiplexing for next generation wireless communications," *IEEE Transactions on Wireless Communications*, vol. 22, no. 11, pp. 8214–8233, 2023.

[7] E. Basar, "Reconfigurable intelligent surfaces for Doppler effect and multipath fading mitigation," *Frontiers in Communications and Networks*, vol. 2, 2021.

[8] C. L. et al., "Reconfigurable intelligent surface-assisted AFDM for high-mobility communications," *International Journal of Electronics and Communications (AEÜ)*, vol. 177, p. 155416, 2025.

[9] H. Y. Kwon, S. M. Kim, and J. W. Choi, "Enhancing integrated sensing and communication with AFDM: soft-information detection over MIMO dispersive channels," *Physical Communication*, vol. 66, p. 102052, 2025.

[10] Y. I. Tek and E. Basar, "A novel and secure AFDM system for high-mobility environments," *IEEE Transactions on Vehicular Technology*, 2025, early Access.

[11] 3GPP, "Physical layer procedures for control (SC-FDMA fundamentals)," 3GPP TS 36.211, Release 15, 2018.

[12] D. Falconer, S. L. Ariyavisitakul, A. Benyamin-Seeyar, and B. Eidson, "Frequency domain equalization for single-carrier broadband wireless systems," *IEEE Communications Magazine*, vol. 40, no. 4, pp. 58–66, 2002.

[13] V. M. Reddy and H. Bitra, "PAPR in AFDM: Upper bound and reduction with normalized μ-law companding," *IEEE Access*, vol. 13, pp. 86 553–86 561, 2025.

Authorized licensed use limited to: Khulna University. Downloaded on October 13,2026 at 09:49:18 UTC from IEEE Xplore. Restrictions apply.